CrystEngComm

PAPER

View Article Online
View Journal | View Issue

Cite this: *CrystEngComm*, 2024, **26**, 2373

Chemical solution deposition of a $(GaAl)_2O_3$ single layer with high thickness and silver-enhanced crystal quality†

Xiao Tang,[a] Wesam A. AlQanbar,[a] Mohamed Ben Hassine,[b] Yi Lu,[a] Haicheng Cao,[a] Chuanju Wang,[a] Zixian Jiang,[a] Tingang Liu,[a] Na Xiao,[a] Mingtao Nong,[a] Vishal Khandelwal[a] and Xiaohang Li*[a]

Received 30th January 2024,
Accepted 8th April 2024

DOI: 10.1039/d4ce00086b

rsc.li/crystengcomm

Traditional chemical solution deposition (CSD) methods for growing Ga_2O_3 films face two main issues: limited thickness per deposition, necessitating multiple coating-annealing cycles for adequate film thickness, and a decline in crystal quality with increased thickness. This study introduces an innovative CSD technique for fabricating $(GaAl)_2O_3$ films, achieving both high thickness and superior crystal quality, where the aluminum content results from the diffusion of aluminum from sapphire substrates during annealing. The technique uses a precursor solution with high viscosity and cation concentration, allowing single-layer thicknesses of up to 180 nm. Additionally, the incorporation of silver nitrate for silver doping enhances nucleation, growth, and epitaxial quality, inducing a unique twelve-fold symmetry in the (−201) oriented $(GaAl)_2O_3$ films. Notably, silver serves as a catalyst and largely evaporates at high temperatures, thus preserving the film's final composition and performance. This study highlights the effectiveness of this CSD approach in simultaneously improving crystal quality and achieving desired film thickness, making it a promising method for mass production of high-quality $(GaAl)_2O_3$ films.

Introduction

Gallium oxide (Ga_2O_3) has recently emerged as a material of significant interest due to its exceptional properties, such as a large bandgap, high breakdown field, and superior thermal stability.[1–5] These characteristics render Ga_2O_3 an ideal candidate for various applications, including power electronics, radio frequency (RF) devices, solar-blind photodetectors, and ozone sensors. It is known that Ga_2O_3 has polymorphs including α, δ, ε, and β phases. Among all the polymorphs, β-Ga_2O_3 stands out due to its superior thermal stability and wider bandgap, thus making it the preferred choice for high-efficiency power electronics and ultraviolet optoelectronic applications.[1] The predominant methods for fabricating high-quality Ga_2O_3 thin films include pulsed laser deposition (PLD), metal–organic chemical vapor deposition (MOCVD), and molecular beam epitaxy (MBE). However, these techniques typically require vacuum conditions.[6–9]

In contrast, chemical solution deposition (CSD) offers a more cost-effective and potentially scalable alternative, suitable for large-scale production, particularly with its compatibility with reel-to-reel systems and possibility of tuning morphology of various nanomaterials.[10–12] Despite its advantages, CSD's main challenge lies in the inferior crystal quality of the films it produces, especially for Ga_2O_3, where the ultra-thin deposition layer (<20 nm) necessitates multiple coating-annealing cycles, making the process time-consuming to achieve the desired thickness.[13–20]

This report introduces an innovative CSD technique designed to address these challenges. The method involves using a novel precursor composed of triethanolamine (TEA), propionic acid, 2-methoxylamine, and gallium nitrate. This precursor achieves a high viscosity (~12 Pa s) and a high cation concentration (2 M), which are crucial for achieving thicker single-layer depositions. However, a thicker layer often compromises epitaxial quality. To mitigate this, silver nitrate is incorporated into the precursor for silver doping. This addition significantly enhances the nucleation and growth of Ga_2O_3, thereby improving the crystallinity and epitaxy of the films. Interestingly, silver doping has been found to induce a unique twelve-fold symmetry in the (−201) oriented Ga_2O_3 films on *c*-plane sapphire substrates. Furthermore, silver acts as a catalyst since it is found to evaporate at high temperatures thus doesn't affect the

[a] *Advanced Semiconductor Laboratory, Electrical, and Computer Engineering Program, CEMSE Division, King Abdullah University of Science and Technology (KAUST), Thuwal, 23955-6900, Saudi Arabia. E-mail: xiaohang.li@kaust.edu.sa*
[b] *Core Labs, King Abdullah University of Science and Technology (KAUST), Thuwal, 23955-6900, Saudi Arabia*

† Electronic supplementary information (ESI) available. See DOI: https://doi.org/10.1039/d4ce00086b

composition and the performance of the films. It is worth mentioning that aluminum diffuses from sapphire substrates during annealing into the Ga_2O_3 films, resulting in a 15–25 atm% aluminum content in the films, leads to the films being more accurately termed as $(GaAl)_2O_3$. However, this diffusion is a common occurrence in high-temperature annealed Ga_2O_3 films on sapphire substrates, thus does not detract from the benefits of the novel CSD method described in this report. In summary, this innovative approach effectively addresses the challenges of achieving superior crystal quality and adequate film thickness in $(GaAl)_2O_3$ deposition, presenting a comprehensive solution for high-quality film production.

Experimental

For preparing the precursor solution with a silver to gallium mole ratio of 0.3, 1 gram of gallium nitrate hydrate (purity 99.9%) was initially dissolved in a solvent mixture containing 2 mL of 2-methyl 1-propanol and 300 μL of triethanolamine. This mixture was stirred vigorously at 60 °C for 2 hours. Subsequently, 0.2 grams of silver nitrate (99.9% pure) was introduced into the solution, which turned transparently clear after 30 minutes. To stabilize the solution, 50 μL of propionic acid was added. The solution's viscosity was recorded at ~12 Pa s using a Kyoto Electronics EMS 1000 viscometer. In contrast, the viscosity of the precursor solution using the conventional recipe has a much lower viscosity of only 2.5 Pa s.[14] The experimental details for the conventional recipe and the viscosity results are shown in ESI.†[14]

The solution was then spin-coated on a 1 cm × 1 cm sapphire substrate, pre-treated at 500 °C for an hour to enhance wetting properties, at 3000 rpm for 1 minute. The coated films were then annealed in a tube furnace, gradually heated to 1100 °C at a rate of 10 °C min^{-1} and maintained at this temperature for two hours before cooling down naturally.

Material phases, in-plane and out-of-plane quality, and high-temperature *in situ* phase evolution of the films were characterized using a Bruker D8 Advance XRD with Cu Kα radiation (λ = 1.5406 Å). Surface morphology was examined using a Dimension Edge atomic force microscope (AFM) from Bruker using tapping mode. High-resolution TEM lamellas of the film samples were prepared with an FEI Helios G4 dual-beam focused ion beam scanning electron microscope system, using a Ga source and omni-probe. HR-TEM images and fast Fourier transform (FFT) patterns of the interfaces were acquired on a Titan ST microscope (FEI, USA) operating at 300 keV. UV–vis spectra were recorded using a Lambda 950 UV/vis/NIR spectrophotometer from PerkinElmer. Differential scanning calorimetry (DSC) and thermogravimetric analysis (TGA) were carried out using a Netzsch STA 449C thermal analyzer in a humid oxygen atmosphere from RT to 1200 °C, at a heating rate of 10 °C min^{-1}. Scanning electron microscopy (SEM) characterization was performed in a LEO 1530 with an in-lens detector (EHT = 10 keV).

Results and discussion

To investigate the impact of silver on gallium oxide films, we introduced silver nitrate ($AgNO_3$) into the precursor solution at an Ag : Ga ratio of 0.3. This approach resulted in a silver doping concentration of 30% in the precursor film post-spin coating. Subsequently, both silver doped and undoped films were annealed at 1100 °C in an air atmosphere for two hours. It should be emphasized that the diffusion of aluminum from the sapphire substrates into the Ga_2O_3 during annealing is a widely reported common process, unrelated to the silver doping process discussed in this report. However, for greater precision, the films are more aptly referred to as $(GaAl)_2O_3$ films. For ease of reference, the silver-doped films will be abbreviated as GAS, while the undoped films will be denoted as GA in subsequent discussions. X-ray diffraction analysis, as illustrated in Fig. 1(a), revealed distinctive differences between the two samples. The GA film exhibited relatively weak diffraction peaks at the (−201) orientation and a peak at the (400) orientation, indicative of random orientation, at approximately 30°. The comparable intensities of these peaks suggest a decline in epitaxial quality at this film thickness, aligning with observations reported in prior studies. In contrast, the GAS sample predominantly displayed intensified (−201) orientation peaks, with the absence of random orientation peaks. Notably, despite the 30% silver doping, there was no observable shift in the (−201) peaks nor any evidence of metallic silver, underscoring the uniform incorporation of silver in the film structure.

Further assessments of crystalline quality using rocking curve and phi-scan techniques were conducted on both GA and GAS films. Due to poor crystallization in the GA sample, no significant signals were detected. As such, only results from the GAS sample are presented in Fig. 1(b) and (c). The rocking curve of the GAS sample demonstrated a full width at half maximum (FWHM) of approximately 0.7°, comparable to the Ga_2O_3 films produced by vacuum-based methods such as HVPE, sputter, PLD and MOCVD, as summarized in Table 1.[21–24] Then the phi-scan was performed by fixing the Bragg angle and tilt angles at 15.38° and 20.36°, respectively. Intriguingly, the phi-scan of the GAS sample exhibited a unique pattern of twelve evenly distributed peaks, each separated by 30°. This distribution contrasts with the six-peak pattern typical of Ga_2O_3 films conventionally deposited on sapphire substrates, which is attributed to three rotationally aligned domains on the sapphire (0001) plane.[25,26] The underlying mechanism of this divergence will be discussed subsequently.

Additionally, AFM images of the GA and GAS samples (Fig. 1(d) and (e)) reveal a noticeably smoother surface texture in the GAS sample compared to the GA sample, highlighting the role of silver doping in modifying surface morphology.

Fig. 2(a) presents the β-$(GaAl)_2O_3$ structure visualized along the [010] direction, with the (−201) plane distinctly highlighted by a dashed gray line. Figure (b) illustrates the conventionally observed relationship between the three

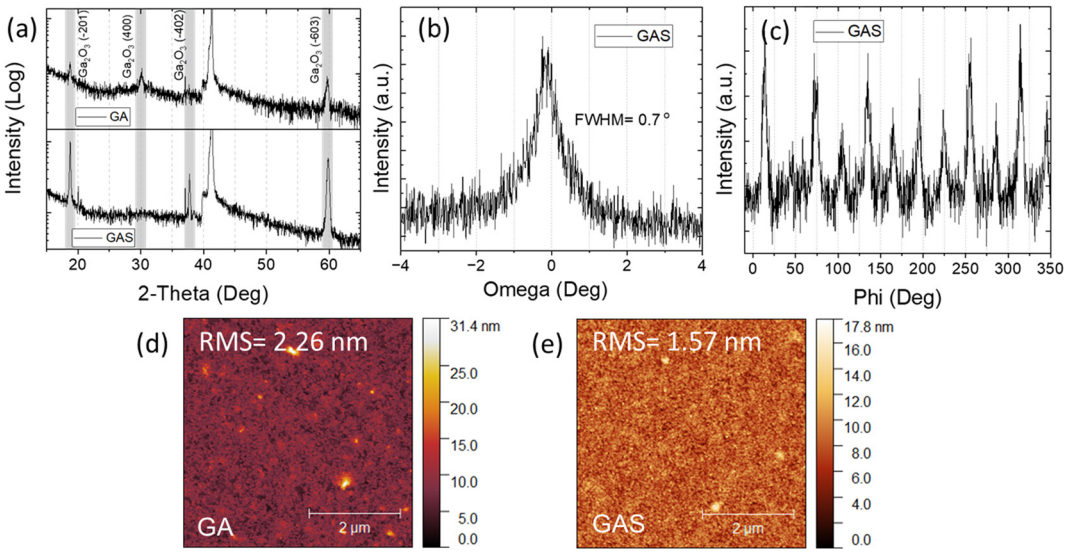

Fig. 1 XRD 2-theta pattern for the sample GA and GAS (a); rocking curve for the sample GAS (b); phi-scan for the sample GAS (c); AFM images for the sample GA (d) and GAS (e).

domains of β-$(GaAl)_2O_3$ (−201) and sapphire (0001), which is attributed to a relatively small lattice mismatch of 10.6%.[26] In our study, the phi-scan revealed an additional set of six peaks. These peaks suggest the presence of another set of three domains of β-$(GaAl)_2O_3$ on sapphire (0001), aligned with an in-plane orientation of <010> β-$(GaAl)_2O_3$ parallel to <110> sapphire, as shown in Fig. 2(c). Although X-ray diffraction (XRD) results show no lattice expansion in the β-$(GaAl)_2O_3$, this alignment is still plausible. Calculations based on the triple lattice distance of β-$(GaAl)_2O_3$ <−201> and the single distance of sapphire <110> yield a lattice mismatch of 10.3%.[27]

To explore the impact of silver on $(GaAl)_2O_3$ crystallization, we conducted high-temperature *in situ* X-ray diffraction (XRD) analyses on both GA (undoped) and GAS (silver-doped) samples, gradually increasing the temperature from 600 °C to 1200 °C. Fig. 3(a) and (b) display the temperature-dependent evolution of the (−201) diffraction peak intensity for GA and GAS, respectively, with both images scaled identically for comparative purposes. It is noticed that both the GA and GAS samples exhibited a shift towards higher angles at a consistent level, attributable to the aluminum diffusion from sapphire to all the two films regardless of silver doping. Additionally, Fig. 3(c) presents the extracted intensity data of the (−201) peak for both samples. A notable observation is the delayed appearance of the (−201) peak in the GA sample, only emerging at around 1000 °C, indicative of a slow crystallization process for undoped β-$(GaAl)_2O_3$. In stark contrast, the GAS sample demonstrates an earlier onset of the (−201) peaks at approximately 800 °C, suggesting that silver doping significantly enhances the crystallization process. This acceleration can be attributed to the inclusion of Ag in the metal-oxide system, which effectively lowers the peritectic temperature.[28–33] This alteration transitions the reaction mechanism from a solid–solid to a solid–liquid state, thereby increasing the mobility of the reactants.

Table 1 Comparison of FWHM values of Ga_2O_3 films using various deposition techniques on sapphire

Deposition technique	FWHM value (deg)	Vacuum requirement	Reference
MOCVD	0.268	Yes	21
HVPE	1.2	Yes	22
PLD	0.26	Yes	23
Sputter	0.35	Yes	24
CSD	0.7	No	This work

Subsequently, thermogravimetric (TG) analysis and differential scanning calorimetry (DSC) measurements were conducted to examine the silver-induced formation of a liquid phase, as depicted in Fig. 4. Initially, TG-DSC evaluations were performed on both pure Ga_2O_3 (comprising $Ga(NO_3)_3$, methyl 1-propanol, triethanolamine) and Ga_2O_3–Ag mixed precursor (including $Ga(NO_3)_3$, $AgNO_3$, methyl 1-propanol, triethanolamine) samples under atmospheric conditions. To ensure the complete evaporation of any residual solvent, all precursor samples were preheated at 120 °C for two hours. As illustrated in Fig. 4(a), both samples exhibited significant weight loss up to 700 °C, attributable to the decomposition of organic compounds. Notably, the sample with silver exhibited a pronounced endothermic peak above 800 °C without concurrent weight loss, signaling the emergence of a liquid phase in the mixed sample. Furthermore, the silver-enriched sample demonstrated greater weight reduction throughout the temperature range examined. The decomposition of gallium nitrate and silver nitrate proceeds according to the reactions below, resulting in weight losses of 63.4% and 36.4%, respectively:

$$4Ga(NO_3)_3(s) \rightarrow 2Ga_2O_3(s) + 12NO_2(g) + 3O_2(g) + 3O_2(g)$$

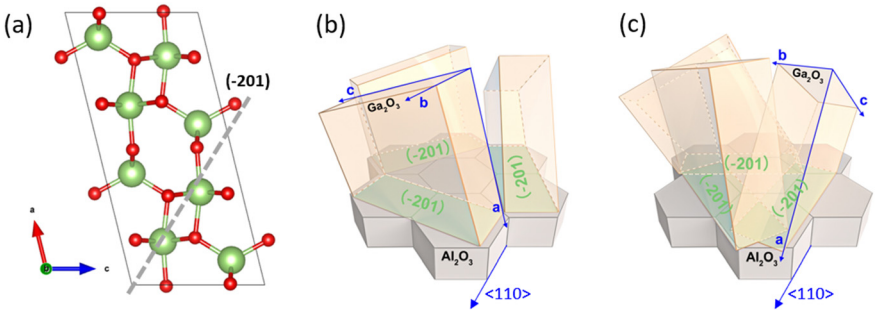

Fig. 2 Illustration of the β-$(GaAl)_2O_3$ crystal structure as viewed along the [010] direction, with the (−201) plane marked by a dashed gray line (a); domain alignment in β-$(GaAl)_2O_3$ and sapphire: a depiction of the positional relationship between the three domains of β-$(GaAl)_2O_3$ (−201) and sapphire (0001), showcasing the orientation alignment of <010> β-$(GaAl)_2O_3$ parallel to <110> sapphire (b), and another three domain alignment, illustrating the orientation of <−201> β-$(GaAl)_2O_3$ parallel to <110> sapphire (c).

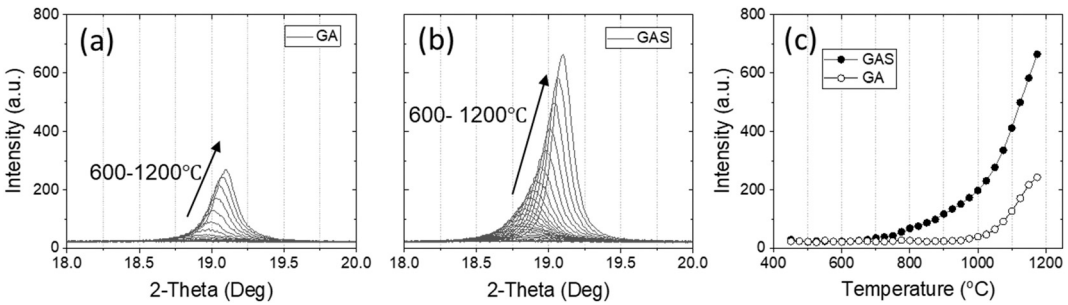

Fig. 3 Evolution of the β-$(GaAl)_2O_3$ (−201) diffraction peak with temperature increase from 600 °C to 1200 °C for GA (a) and GAS (b); corresponding intensity variation of the β-$(GaAl)_2O_3$ (−201) peak as a function of temperature for GA and GAS (c).

$$2AgNO_3(s) \rightarrow 2Ag(s) + 4NO_2(g) + O_2(g)$$

Theoretically, the presence of silver nitrate in the precursor should result in a lower overall weight loss. However, experimental findings reveal the contrary, suggesting an intriguing anomaly in the behavior of the mixed samples. To understand the higher weight loss for the silver added sample, another measurement was performed. In this measurements, Ga_2O_3, Ag, and Ga_2O_3–Ag solid samples were prepared by heating the corresponding precursor samples in a furnace at 600 °C in air for one hour to remove all the organic compounds then subjected to the TG measurements. The findings indicate that the silver-added sample undergoes weight loss more readily than the pure Ga_2O_3 sample, while the pure silver sample exhibits substantial weight loss at temperatures exceeding 1000 °C. These observations imply that silver undergoes evaporation at elevated temperatures. Similar findings were also described in some other reports that can be found elsewhere.[34,35] And it is noted that in the TG measurements, powder mixtures are used for the investigated materials, which however, have a lower effective surface area exposed to the environment, especially if the particles are agglomerated or clumped together. In contrast, in the actual thin film, the materials has a higher surface area exposed to the environment compared to its volume. This increased surface area can enhance the rate of sublimation as more metal atoms are at the surface and can escape into the gas phase. This means that in the thin films the weight loss can be happened at a much lower temperature compared to the temperatures observed in the TG measurements.

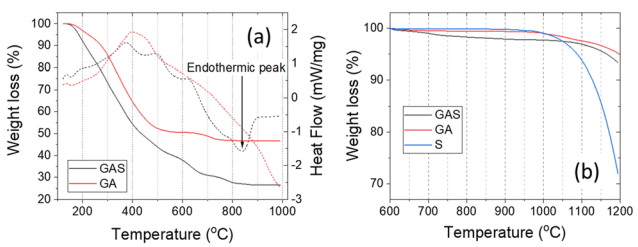

Fig. 4 (a) Thermogravimetric (TG) analysis and differential scanning calorimetry (DSC) plots for the gallium oxide (Ga_2O_3) precursor (GA) and the gallium oxide-silver (Ga_2O_3–Ag) mixed precursor (GAS), with solid lines depicting TG data and dashed lines indicating DSC data. (b) Detailed TG analysis of solid gallium oxide (GA), a mixture of gallium oxide and silver oxide (GAS), and pure silver oxide (S).

The crystallization of β-$(GaAl)_2O_3$ on a sapphire substrate aligns with the heterogeneous nucleation model, described by the following formula:[36]

$$\Delta G^*_{\text{hetero}} = \frac{16\pi r^3}{3(\Delta G_V)^2}\left[\frac{2-3\cos\theta+\cos^3\theta}{4}\right] \quad (1)$$

where $\Delta G^*_{\text{hetero}}$ represents the critical Gibbs free energy change for heterogeneous nucleation. It's the energy barrier that must be overcome for a stable nucleus (the initial form of a new phase) to form on a surface different from the bulk material, r is the radius of the

nucleus, ΔG_V represents the volume free energy change. It's the difference in Gibbs free energy per unit volume between the new phase and the old phase, and θ is the contact angle between the nucleus and the substrate. It's a measure of how well the new phase "wets" the substrate. A small contact angle indicates good wetting. It is therefore deduced that when silver facilitate the formation of peritectic phase with gallium contents, the created liquid phase will largely decrease the contact angle between the reactants in the precursor film and the sapphire substrate, thereby making the energy barrier significantly decreased. As a result, the β-$(GaAl)_2O_3$ can form at a much lower temperature due to the presence of silver. In such a "liquid–solid" reaction scenario, the presence of a liquid phase enhances atomic or molecular mobility compared to a solid phase, thus promoting the emergence of new crystalline domains in diverse orientations. As such, we believe that the observed in-plane rotation of the β-$(GaAl)_2O_3$ films is also related to the liquid formation. While the sapphire lattice continues to dominate the out-of-plane orientation, aligning the β-$(GaAl)_2O_3$ grains along the <−201> direction, the liquid phase serves as a conducive medium for atoms to diffuse and nucleate in varied in-plane orientations. This process potentially leads to the observed additional in-plane orientations. For the pure Ga_2O_3 sample, the energy barrier for nucleation, with an in-plane orientation of <010> β-$(GaAl)_2O_3$ aligned to <110> sapphire, is lower than for <−201> β-$(GaAl)_2O_3$ aligned to <110> sapphire. Consequently, the former orientation predominates over the latter. However, with the addition of silver, the liquid phase formation significantly reduces the discrepancy in energy barriers between the two orientations, allowing both orientations to occur simultaneously.

Fig. 5(a) presents a large-scale transmittance electron microscopy (TEM) image, displaying a thickness of approximately 180 nm. This value significantly exceeds the thickness typical for single layers applied *via* conventional precursor solutions, as detailed in other studies.[14] Fig. 5(b) offers a high-resolution TEM image, in which the positions of the atoms correspond quite well to those in the beta-phase β-$(GaAl)_2O_3$. Fig. 5(c) reveals the corresponding Fast Fourier Transform (FFT) analysis, also demonstrates the formation of β-$(GaAl)_2O_3$. Fig. 5(d)–(h) focus on zoomed-in TEM images, complemented with energy-dispersive X-ray spectroscopy (EDX) patterns for oxygen, gallium, aluminum, and silver, respectively. Notably, aluminum appears to have diffused from the sapphire substrate into the β-$(GaAl)_2O_3$ film, resulting in an aluminum composition in a range of 15–25%. Such a phenomenon is extensively reported in our prior research.[37] Despite incorporating 30% silver into the metal–organic precursor solution, post-sintering EDX analyses reveal only a minuscule presence of silver in the β-$(GaAl)_2O_3$ film at the grain boundaries as shown in Fig. 5(h). SEM images and EDX pattern were also taken on the surface of the sample GA and GAS as shown in Fig. S2.† It also confirms that no silver signal was detected, suggesting a removal of silver during annealing.

Fig. 6 illustrates the Tauc plot depicting the variation of $(\alpha h\nu)^2$ against photon energy for β-$(GaAl)_2O_3$ thin films synthesized from precursor solutions with varying silver contents. This plot shows that the photon energy required

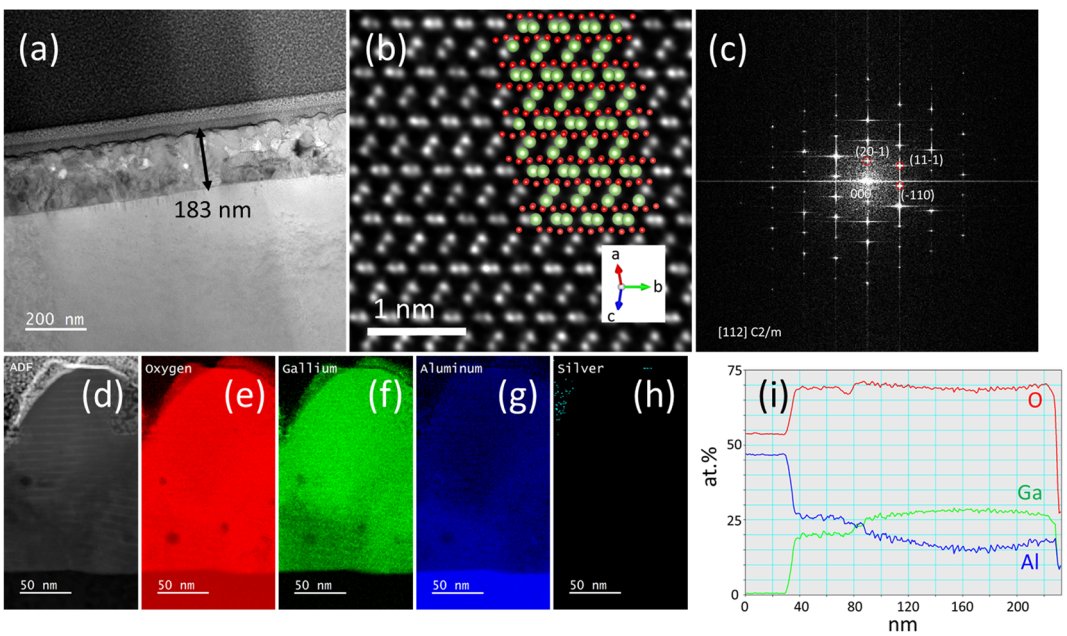

Fig. 5 Large-scale transmittance electron microscopy (TEM) image (a), high-resolution TEM image (b), and the corresponding FFT pattern (c) of single GAS layer, respectively, where the inset in (b) shows the atom distributions of gallium (green dots) and oxygen (red dots); (d) to (h) provide zoomed-in TEM images with energy-dispersive X-ray spectroscopy (EDX) for oxygen, gallium, aluminum, and silver; distribution of atoms of oxygen, gallium, and aluminum percentages across the film's thickness (i).

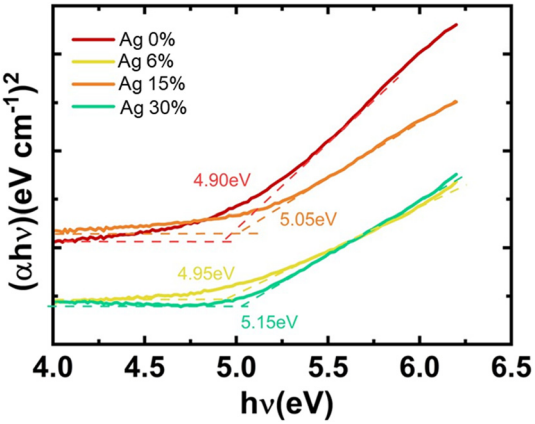

Fig. 6 Tauc plot of $(\alpha h\nu)^2$ as a function of the photon energy for β-$(GaAl)_2O_3$ thin films derived from precursor solution with different silver content.

increases with the addition of silver compared to films produced from silver-free precursor solutions. Notably, at a high silver content of 30%, the photon energy shift is relatively minor, at only 0.25 eV. This suggests that while traces of silver might remain in the β-$(GaAl)_2O_3$ films, the majority of the silver likely evaporates due to sublimation during the high-temperature annealing process.

Conclusion

In summary, we developed an innovative CSD technique for fabricating high-quality β-$(GaAl)_2O_3$ thin films. It introduces a novel precursor solution with high viscosity and cation concentration, enabling thicker single-layer depositions. Silver doping is incorporated to enhance nucleation, growth, and epitaxy of β-$(GaAl)_2O_3$ films. Studies reveal that silver doping leads to unique crystalline properties and surface morphology, and aids in lowering the peritectic temperature, transitioning from a solid–solid to a solid–liquid state reaction. This facilitates diverse crystalline domain orientations and enhances film quality, while most of the silver evaporates during high-temperature annealing, leaving minimal trace in the films.

Conflicts of interest

There are no conflicts to declare.

Acknowledgements

This work was supported by KAUST Baseline Fund: BAS/1/1664-01-01, KAUST Near-term Grand Challenge Fund: REI/1/4999-01-01, KAUST Impact Acceleration Fund: REI/1/5124-01-01.

References

1 S. J. Pearton, *et al.*, A review of Ga2O3 materials, processing, and devices, *Appl. Phys. Rev.*, 2018, **5**(1), 011301.
2 Z. Liu, *et al.*, Comparison of optoelectrical characteristics between Schottky and Ohmic contacts to β-Ga2O3 thin film, *J. Phys. D: Appl. Phys.*, 2020, **53**(8), 085105.
3 Y. Lu, *et al.*, Ultrasensitive Flexible kappa-Phase Ga(2)O(3) Solar-Blind Photodetector, *ACS Appl. Mater. Interfaces*, 2022, **14**(30), 34844–34854.
4 S. Yuvaraja, *et al.*, Wide bandgap semiconductor-based integrated circuits, *Chip*, 2023, **2**, 100072.
5 V. Khandelwal, *et al.*, Demonstration of β-Ga2O3 nonvolatile flash memory for oxide electronics, *Jpn. J. Appl. Phys.*, 2023, **62**(6), 060902.
6 X. Tang, *et al.*, Quasi-Epitaxial Growth of beta-Ga(2)O(3)-Coated Wide Band Gap Semiconductor Tape for Flexible UV Photodetectors, *ACS Appl. Mater. Interfaces*, 2022, **14**(1), 1304–1314.
7 X. Tang, *et al.*, Epitaxial growth of β-Ga2O3 (−201) thin film on four-fold symmetry CeO2 (001) substrate for heterogeneous integrations, *J. Mater. Chem. C*, 2021, **9**(44), 15868–15876.
8 A. Hernandez, *et al.*, MOCVD growth and characterization of conductive homoepitaxial Si-doped Ga2O3, *Results Phys.*, 2021, 25.
9 T. Hadamek, *et al.*, β-Ga2O3 on Si (001) grown by plasma-assisted MBE with γ-Al2O3 (111) buffer layer: Structural characterization, *AIP Adv.*, 2021, **11**(4), 045209.
10 K. Chen, S. Song and D. Xue, Chemical reaction-controlled synthesis of Cu2O hollow octahedra and core–shell structures, *CrystEngComm*, 2013, **15**, 10028–10033.
11 K. Chen and D. Xue, Chemo affinity-mediated crystallization of Cu2O: a reaction effect on crystal growth and anode property, *CrystEngComm*, 2013, **15**, 1739–1746.
12 K. Chen and D. Xue, pH-assisted crystallization of Cu2O: chemical reactions control the evolution from nanowires to polyhedral, *CrystEngComm*, 2012, **14**, 8068–8075.
13 G. S. Cai, Y. L. Pei and S. D. Zhang, Investigation of Solution-Processed Ga2O3 Thin Films and their Application in Dielectric Materials, *Mater. Sci. Forum*, 2020, **1014**, 27–32.
14 H. Shen, *et al.*, Growth and characterization of β-Ga2O3 thin films by sol-gel method for fast-response solar-blind ultraviolet photodetectors, *J. Alloys Compd.*, 2018, **766**, 601–608.
15 X. Tang, *et al.*, Chemical solution deposition of epitaxial indium- and aluminum-doped Ga2O3 thin films on sapphire with tunable bandgaps, *J. Eur. Ceram. Soc.*, 2022, **42**(1), 175–180.
16 Y. Ohya, *et al.*, Fabrication of Ga2O3 thin films by aqueous solution deposition, *J. Ceram. Soc. Jpn.*, 2009, **117**, 972–977.
17 Y. Kokubun, L. Miura, F. Endo and S. Nakagomi, Sol-gel prepared thin films for ultraviolet Photodetectors, *Appl. Phys. Lett.*, 2007, **90**, 031912.
18 M. Bartic, M. Ogita and M. Isai, Oxygen sensing properties at high temperatures of Ga2O3 thin films deposited by the chemical solution deposition method, *Appl. Phys. Lett.*, 2007, **102**, 023709.
19 L. Yuan, S. Li, G. Song, X. Sun and X. Zhang, Solution-processed amorphous gallium oxide gate dielectric for low-

voltage operation oxide thin film transistors, *J. Mater. Sci.: Mater. Electron.*, 2021, **32**, 8347–8835.

20 W. Xu, H. Cao, L. Liang and J. Xu, Aqueous Solution-Deposited Gallium Oxide Dielectric for Low-Temperature, Low-Operating-Voltage Indium Oxide Thin-Film Transistors: A Facile Route to Green Oxide Electronics, *ACS Appl. Mater. Interfaces*, 2015, **7**, 14720–14725.

21 R.-H. Horng, D.-S. Wuu, P.-L. Liu, A. Sood, F.-G. Tarntair, Y.-H. Chen, S. J. Pratap and C.-L. Hsiao, Growth mechanism and characteristics of β-Ga2O3 heteroepitaxailly grown on sapphire by metalorganic chemical vapor deposition, *Mater. Today Adv.*, 2022, **16**, 100320.

22 G. Pozina, C. W. Hsu and N. Abrikossova, *et al.*, Development of β-Ga2O3 layers growth on sapphire substrates employing modeling of precursors ratio in halide vapor phase epitaxy reactor, *Sci. Rep.*, 2020, **10**, 22261.

23 C. Wang and S.-W. Li, *et al.*, Structural, optical and morphological evolution of Ga2O3/Al2O3 (0001) films grown at various temperatures by pulsed laser deposition, *Ceram. Int.*, 2021, **47**(21), 29748–29757.

24 W. Cui and Q. Ren, *et al.*, Optimization of Growth Temperature of β-Ga2O3 Thin Films for Solar-Blind Photodetectors, *J. Nanosci. Nanotechnol.*, 2017, **17**, 1–6.15.

25 W. Seiler, *et al.*, Epitaxial growth of gallium oxide films on c-cut sapphire substrate, *Thin Solid Films*, 2015, **589**, 556–562.

26 S. Nakagomi and Y. Kokubun, Crystal orientation of β-Ga2O3 thin films formed on c-plane and a-plane sapphire substrate, *J. Cryst. Growth*, 2012, **349**(1), 12–18.

27 Y. Chen, *et al.*, The lattice distortion of β-Ga2O3 film grown on c-plane sapphire, *J. Mater. Sci.: Mater. Electron.*, 2015, **26**(5), 3231–3235.

28 X. Tang, *et al.*, High-Jc YBa2Cu3O7−x-Ag superconducting thin films synthesized through a fluorine-free MOD method, *J. Eur. Ceram. Soc.*, 2015, **35**(6), 1761–1769.

29 X. Obradors, *et al.*, Nucleation and mesostrain influence on percolating critical currents of solution derived YBa2Cu3O7 superconducting thin films, *Phys. C*, 2012, **482**, 58–67.

30 B. Bian, J. Yie, B. Li and Z. Wu, Fractal formation in a-Si:H/Ag/a-Si:H films after annealing, *J. Appl. Phys.*, 1993, **73**(11), 7402–7406.

31 T. Aoki, H. Kanno, A. Kenjo, T. Sadoh and M. Miyao, Au-induced lateral crystallization of a-Si1−xGex (x: 0–1) at low temperature, *Thin Solid Films*, 2006, **508**, 44–47.

32 L. Hultman, A. Robertsson, H. T. G. Hentzell, I. Engström and P. A. Psaras, Crystallization of amorphous silicon during thin-film gold reaction, *J. Appl. Phys.*, 1987, **62**(9), 3647–3655.

33 X. Tang, Y. Zhao and W. Wu, *et al.*, Effect of BaZrO3/Ag hybrid doping to the microstructure and performance of fluorine-free MOD method derived Yba2Cu3O7−x superconducting thin films, *J. Mater. Sci.: Mater. Electron.*, 2015, **26**, 1806–1811.

34 Y. Ding, *et al.*, Sublimation-Induced Shape Evolution of Silver Cubes, *Small*, 2009, **5**(24), 2812–2815.

35 C. Hong, *et al.*, Effect of silver content on the microstructure, thermal stability and mechanical properties of CrNx/Ag nanocomposite films, *Ceram. Int.*, 2021, **47**, 25324–25336.

36 Y. Chen, *et al.*, Growth Pressure Controlled Nucleation Epitaxy of Pure Phase ε- and β-Ga2O3 Films on Al2O3 *via* Metal–Organic Chemical Vapor Deposition, *Cryst. Growth Des.*, 2018, **18**(2), 1147–1154.

37 C.-H. Liao, *et al.*, Wide range tunable bandgap and composition β-phase (AlGa)2O3 thin film by thermal annealing, *Appl. Phys. Lett.*, 2021, **118**(3), 032103.